Ann. Geophys., 35, 1309–1326, 2017
https://doi.org/10.5194/angeo-35-1309-2017

Annales Geophysicae Open Access EGU

Total electron content responses to HILDCAAs and geomagnetic storms over South America

Patricia Mara de Siqueira Negreti, Eurico Rodrigues de Paula, and Claudia Maria Nicoli Candido

Aeronomy Division, National Institute for Space Research, INPE, São José dos Campos, Brazil

Correspondence to: Patricia Mara de Siqueira Negreti (psiqueira.negreti@gmail.com)

Received: 21 June 2017 – Revised: 16 September 2017 – Accepted: 31 October 2017 – Published: 7 December 2017

Abstract. Total electron content (TEC) is extensively used to monitor the ionospheric behavior under geomagnetically quiet and disturbed conditions. This subject is of greatest importance for space weather applications. Under disturbed conditions the two main sources of electric fields, which are responsible for changes in the plasma drifts and for current perturbations, are the short-lived prompt penetration electric fields (PPEFs) and the longer-lasting ionospheric disturbance dynamo (DD) electric fields. Both mechanisms modulate the TEC around the globe and the equatorial ionization anomaly (EIA) at low latitudes. In this work we computed vertical absolute TEC over the low latitude of South America. The analysis was performed considering HILDCAA (high-intensity, long-duration, continuous auroral electrojet (AE) activity) events and geomagnetic storms. The characteristics of storm-time TEC and HILDCAA-associated TEC will be presented and discussed. For both case studies presented in this work (March and August 2013) the HILDCAA event follows a geomagnetic storm, and then a global scenario of geomagnetic disturbances will be discussed. Solar wind parameters, geomagnetic indices, O / N_2 ratios retrieved by GUVI instrument onboard the TIMED satellite and TEC observations will be analyzed and discussed. Data from the RBMC/IBGE (Brazil) and IGS GNSS networks were used to calculate TEC over South America. We show that a HILDCAA event may generate larger TEC differences compared to the TEC observed during the main phase of the precedent geomagnetic storm; thus, a HILDCAA event may be more effective for ionospheric response in comparison to moderate geomagnetic storms, considering the seasonal conditions. During the August HILDCAA event, TEC enhancements from ~ 25 to 80 % (compared to quiet time) were observed. These enhancements are much higher than the quiet-time variability observed in the ionosphere. We show that ionosphere is quite sensitive to solar wind forcing and considering the events studied here, this was the most important source of ionospheric responses. Furthermore, the most important source of TEC changes were the long-lasting PPEFs observed on August 2013, during the HILDCAA event. The importance of this study relies on the peculiarity of the region analyzed characterized by high declination angle and ionospheric gradients which are responsible for creating a complex response during disturbed periods.

Keywords. Ionosphere (equatorial ionosphere)

1 Introduction

The complex effects of magnetospheric convection in ionospheric electric fields and currents from middle to low latitudes during geomagnetic disturbances have been documented in several studies (Blanc, 1983; Heelis and Coley, 1992; Fejer, 1997; Foster and Rich, 1998; Kelley et al., 1979, 2003, 2010; Huang et al., 2005a, b; Mannucci et al., 2008, 2009; Tsurutani et al., 2008a, b; de Siqueira et al., 2011). Under geomagnetically disturbed conditions, the two main sources of electric fields responsible for changes in the plasma drifts and for current perturbations are the prompt penetration electric fields (PPEFs) and the long-lasting ionospheric disturbance dynamo (DD) electric fields. The changes in the equatorial ionization anomaly (EIA) are one of the most perceptible responses of the equatorial thermosphere–ionosphere system to the magnetospheric disturbances (Abdu et al., 1993). These changes can be caused by modifications in the ionospheric electric fields and also by thermospheric winds (Prölss, 1995). The EIA is attributed to the so-called fountain effect which is caused by the vertical $E \times B$ drift. The disturbed electric fields at ionosphere during

active times and geomagnetic storms lead to large changes in dayside total electron content (TEC) at low and middle latitudes and the physical mechanisms involved in these changes are well understood (Fuller-Rowell et al., 1997; Tsurutani et al., 2004a, 2007, 2008a, b; Huba et al., 2005; Lin et al., 2005).

The PPEF events were at first deduced from their consequent magnetic field observed in the equatorial electrojet (Nishida, 1968). Several researchers observed that the interplanetary electric field (IEF) could penetrate into the magnetosphere–ionosphere system (Reddy et al., 1979; Kelley et al., 1979). Some studies (Huang et al., 2005a, b; Mannucci et al., 2005; Tsurutani et al., 2004a, 2008a) proposed a long-duration prompt penetration of IEF into ionosphere during large southward incursions of IMF B_z and a large uplift of ionospheric plasma with a resulting enhanced TEC on the EIA crests. Also, Tsurutani et al. (2008a) proposed the idea of penetration of the dusk-to-dawn IEF, i.e., during northward IMF B_z turnings. Generally, the PPEFs have typical rise and decay shorter than about 15 min duration, and lifetimes of about 1 h (Gonzales et al., 1979; Fejer, 1986).

The ionospheric disturbance dynamo is due to the dynamic action of thermospheric winds produced by auroral heating during the storm time. These winds modify the global circulation generating disturbed ionospheric electric fields at middle and low latitudes (Blanc and Richmond, 1980) and cause variations in thermospheric composition and densities (Rishbeth, 1975). The DD electric fields have timescales from ~ 2 h to ~ 30 h (Fejer and Scherliess, 1997; Scherliess and Fejer, 1997). The quiet-time zonal electric field at ionosphere has an eastward (westward) polarity during the day (night), while the DD electric field points westward in the dayside and eastward at nightside; thus, during the action of DD mechanism the eastward component of the quiet zonal electric field tends to diminish or even reverse. From the EIA development point of view, the action of DD electric fields tends to diminish the vertical $E \times B$ drift and the fountain effect, resulting in a weaker EIA (with lower TEC on the crests), or even to reverse the fountain effect.

In this work we will report on the ionospheric response to two geomagnetic storms followed by high-intensity, long-duration, continuous auroral electrojet (AE) activity (HILDCAA) events. Several studies regarding this topic have been published and some also show the low-latitude responses (Tsurutani et al., 2004b, 2006; Sobral et al., 2006; Koga et al., 2011). Tsurutani and Gonzalez (1987) proposed some empirical definitions in order to establish the HILDCAA occurrence: (a) AE index must reach peaks greater than or equal to 1000 nT sometime during the event, (b) the event must have a duration of at least 2 days, (c) AE never drops below 200 nT for more than 2 h at a time, and (d) the auroral activity occurs outside the main phase of magnetic storms. Tsurutani et al. (2004b) argued that the original criteria set for HILDCAA events was arbitrary and extreme criteria were also imposed to illustrate the phenomena. They state that HILDCAAs may occur even if one or more of these criteria are not followed. HILDCAAs are caused by corotating high-speed solar streams (HSSs) emanating from coronal holes which are more frequent during the declining phase of the solar cycle (Tsurutani et al., 1995). Additionally, the interaction between HSSs and slower-speed streams (near the ecliptic plane) is responsible for creating regions of intense magnetic field called "corotating interaction regions" or CIRs (Tsurutani et al., 2004b, 2006, and references therein). The impingement of CIRs at the magnetosphere can cause CIR-induced geomagnetic storms of weak to moderate intensity, which are followed by HILDCAAs periods (days to weeks) when elevated levels of the ring current are observed (Dst). One characteristic of a CIR-induced storm can be a long recovery phase. While the CIR is responsible for the main phase of a magnetic storm, the following HSS is responsible for the long-duration recovery phase which is characterized by HILDCAA events. The recovery phase of a CIR-induced geomagnetic storm is quite different from that caused by an ICME (interplanetary coronal mass ejection). The HILDCAA phenomena are referred to as magnetospheric/ionospheric events occurring during the continuous impact of solar wind structures consisted of Alfvén waves (Alfvén trains). These Alfvén waves are characterized by subsequent southward incursions of the interplanetary magnetic field (IMF) B_z. These waves favor a strong coupling process and an intermittent magnetic reconnection process between the IMF and the geomagnetic field and cause an increase in the auroral activity denoted by the AE index. Tsurutani et al. (2004b) showed that HILDCAAs are not related to geomagnetic substorms, being an independent phenomenon. Also, they emphasized that the mechanisms responsible for generating HILDCAA events are not the same as those responsible for triggering geomagnetic storms main phases; thus, they can occur even without previous geomagnetic storms. They reported that intense geomagnetic responses related to HILDCAAs can occur after the recovery phases of geomagnetic storms. It is important to emphasize that both PPEFs and disturbance dynamo (DD) electric fields are likely present during a HILDCAA event contributing to a combined ionosphere response during the long recovery phase. Observations of disturbance dynamo electric fields and disturbed winds during HILDCAAs were reported by Sobral et al. (2006) based on digisonde data (hmF2 and foF2) at low latitudes. Mlynczak et al. (2010) and Verkhoglyadova et al. (2011) noted that the variability in NO infrared emissions irradiated from the thermosphere has a good connection with moderate geomagnetic activity during CIR/HSSs and VTEC (vertical TEC) intensification.

Increased auroral energy input due to HSS (reflected in AE indices) and associated heating are likely driven by HILDCAAs. To understand the mechanism of the solar wind–ionosphere coupling during HSSs, Verkhoglyadova et al. (2013) analyzed the role of the PPEF mechanism. They found that there is a correlation between geoeffective IEF

intervals (when it is eastward) and HSS occurrences, and daytime VTEC variability. They suggested that the PPEF is responsible for a prompt (within several hours) ionospheric response during a CIR/HSS interval. There is evidence of prompt equatorial ionospheric response and continuously penetrating IEF (Wei et al., 2008; Koga et al., 2011) during HILDCAAs.

Many studies have presented the ionospheric responses during HSS and HILDCAA considering the solar minimum occurred on 2008–2009, but in this work we intend to show the differences verified between two events of geomagnetic storm followed by HILDCAA occurring during the high solar activity of solar cycle 24 (2013). It is worth mentioning here that the maximum solar activity observed during solar cycle 24 (2013–2014) was of less intensity compared to the previous maximum, occurred on 2000. In this work the solar activity observed in 2013 is referred to as *high*. Our objective is to analyze the HILDCAA responses and the relationship between the HILDCAA event and the precedent geomagnetic storm. Our focus is also to analyze the low-latitude responses over South America.

2 Experimental data

The geomagnetic data and the F10.7 index used in this work were obtained from the low-resolution OMNIWeb database (http://omniweb.gsfc.nasa.gov/form/dx1.html). This database provides the documentation about such geomagnetic and solar indexes. We used the planetary Kp index as indicator of global geomagnetic disturbances and the Sym-H index to verify the phases of the geomagnetic storms. The AE index was analyzed to verify the periods of HILDCAA occurrence. Also, we have used the solar radio flux at 10.7 cm (2800 MHz), namely the F10.7 index, which is an excellent indicator of solar activity and correlates with the sunspot number.

The solar wind plasma and interplanetary magnetic field parameters measured by the ACE satellite were obtained from the high-resolution OMNIWeb database (http://omniweb.gsfc.nasa.gov/form/omni_min.html). This solar wind database has a time delay correction corresponding to the traveling time between the instant of ACE observation and the instant of interaction at the magnetopause. The interplanetary magnetic field (IMF) B_z component is in GSM coordinates. Southward incursions of the IMF B_z are associated with PPEFs and solar wind energy transfer mechanism. The interplanetary electric field (IEF) represents the electric field of the solar wind and is given by $\overrightarrow{E_y} = -\overrightarrow{V_{SWx}} \times \overrightarrow{B_z}$. Positive (negative) E_y is directed approximately duskward (dawnward) in the magnetospheric equatorial plane. It is worth mentioning here that a duskward IEF E_y is related to a southward incursion of the IMF B_z; then, the duskward-oriented E_y is the geoeffective structure for PPEF occurrence (Burton et al., 1975) and energy injection from solar wind through magnetic reconnection (Gonzalez et al., 1994). Considering this, we calculated the geoeffective IEF E_y for penetration of electric field, given by $E_{rec} = V_{SW} B_T [\sin(\theta/2)]^2$, where V_{SW} is the solar wind speed and θ is the "clock angle" between the z axis and the transverse component of the IMF vector $\boldsymbol{B}_T$, ($\boldsymbol{B}_T = B_y + B_z$ in GSM coordinates; Gonzalez et al., 1994). The half-wave rectification of the IEF given by E_{rec} takes into account only the positive (duskward) contribution of IEF E_y (Burton et al., 1975).

In order to verify the occurrence of penetration electric fields, we present magnetometer data given by the ΔH parameter which provide a realistic approximation for the daytime ionospheric zonal electric field at equatorial region since it is related to the equatorial electrojet strength. ΔH is the difference in the magnitudes of the horizontal component of geomagnetic field between a magnetometer placed directly on the magnetic equator and one displaced 6–9° away. In this work we retrieved Jicamarca–Piura ΔH data from Jicamarca Radio Observatory available online at http://jro.igp.gob.pe/database/magnetometer/html/magdata.htm. The basis of this method was first proposed by Rastogi and Klobuchar (1990) and many studies used this methodology to calculate equatorial vertical drifts which are directly proportional to the zonal electric field through the relationship $V_D = E/B$, where V_D is the vertical drift, E is the zonal electric field and B is the magnitude of the geomagnetic field at the point on the geomagnetic equator (Anderson et al., 2002, 2004; Huang et al., 2005b). Since the disturbances in ΔH are related to disturbances in the zonal electric field, the ΔH provides a qualitative manner to verify the occurrence of penetration electric fields in the equatorial ionosphere. The relationship between ΔH and the equatorial vertical drifts is valid only for daytime since the magnetometer measurements are based on the electrojet strength.

The low-latitude TEC presented here was derived from dual-frequency GPS measurements recorded at several arrays installed across the South American continent. The GPS data from International GNSS System (IGS) stations located in South America can be downloaded from Scripps Orbit and Permanent Array Center (SOPAC) Garner GPS archive at http://garner.ucsd.edu. The Brazilian data were retrieved from the Brazilian Network for Permanent Monitoring (RBMC) of the Brazilian Institute of Geography and Statistics (IBGE) at http://www.ibge.gov.br/home/geociencias/download/tela_inicial.php?tipo=8.

The absolute TEC data were generated for each of the GPS receivers using a computational program that was developed at Boston College (Seemala and Valladares, 2011) and provided to be used in this work (C. Valladares, personal communication, 2016). The code uses the GPS observables (pseudo-range and carrier phase) for both L1 (1575.42 MHz) and L2 (1227.60 MHz) GPS frequencies in order to eliminate errors associated with the clock and tropospheric water vapor. The slant and relative TEC (STEC) is calculated based on the established methodology described in

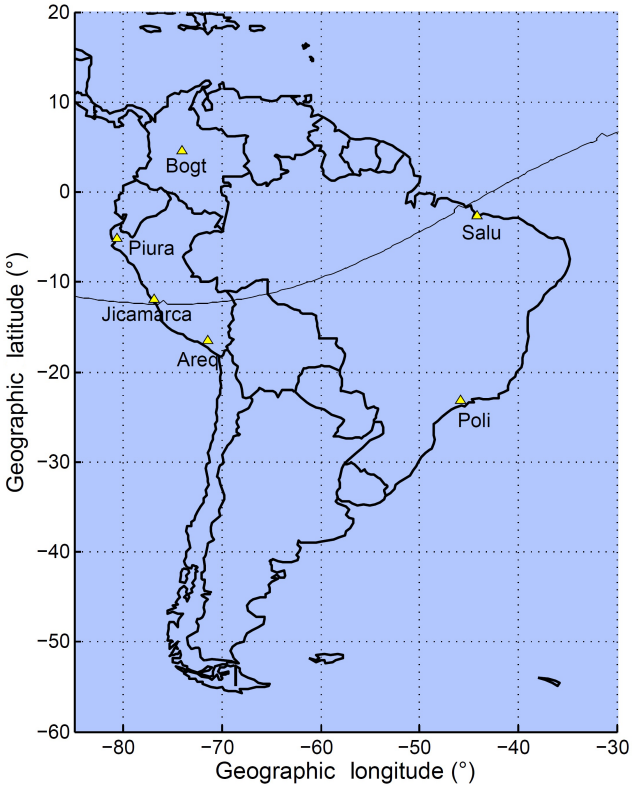

Figure 1. Locations of four GPS stations (Bogt, Areq, Poli, Salu) and two magnetometers (Jicamarca and Piura) used in this work.

Klobuchar (1996) and Sardón and Zarraoa (1997). These relative STEC values contain the differential instrument biases related to the satellite and receiver. The last step is to calculate the absolute vertical TEC (VTEC) values using the relationship $\mathrm{VTEC} = [\mathrm{STEC} - (b_\mathrm{R} + b_\mathrm{S})] / S(E)$, which takes into account the satellite biases (b_S) provided by the University of Bern and the receiver biases (b_R) that are obtained by minimizing the TEC variability between 02:00 and 06:00 LT (Valladares et al., 2009). $S(E)$ is the slant factor used to map slant TEC into vertical TEC and is given by

$$S(E) = \frac{1}{\cos(z)} = \left\{1 - \left(\frac{R_\mathrm{E} \times \cos(E)}{R_\mathrm{E} + h_\mathrm{S}}\right)^2\right\}^{-0.5},$$

where R_E is the mean radius of the Earth in km, h_S is the ionosphere height above the Earth's surface (400 km), z is the zenith angle and E is the elevation angle in degrees. This code was extensively tested and gives appropriate results for South America, as presented in Valladares et al. (2009), Seemala and Valladares (2011) and LISN (Low Latitude Ionospheric Sensor Network) data available at http://lisn.igp.gob.pe.

Table 1 shows the coordinates and local time of all stations used in this study. Figure 1 shows a map containing the locations of these stations.

In order to verify the changes in the neutral atmospheric composition during the disturbances, we will present the Global Ultraviolet Imager (GUVI) data available for the periods analyzed here, obtained at http://guvitimed.jhuapl.edu/. The Global Ultraviolet Imager is one of four instruments that constitute the TIMED spacecraft and provides measurements of daytime O / N_2 ratio at ionospheric F layer heights. TIMED instruments provide useful data regarding the energetics and dynamics of the mesosphere and lower thermosphere between an altitude of approximately 60 to 180 km.

3 Observations and discussion

In this work we show the responses of the low-latitude ionosphere for two HILDCAA and geomagnetic storm events. These events occurred in 2013 (high solar activity for the cycle 24): the first event on 14–31 March, an equinoctial period; the second event on 2–20 August, a transition period from winter solstice to equinox. Although most authors have focused on the solar minimum and descendent solar activity to analyze HSS/CIR and HILDCAAs events when they are more frequent, in this work we intend to discuss their responses to higher solar activity. Our objective is to compare the ionospheric responses considering moderate/intense geomagnetic storms and HILDCAAs and also to verify the effectiveness of both phenomena to generate ionospheric changes at equatorial and low-latitude regions. Data from four GPS stations used to calculate TEC were selected as follows: the geomagnetic equatorial stations Areq and Salu and the EIA crest stations Bogt (north) and Poli (south). These particular locations were chosen to elucidate the local ionospheric response throughout South America.

Before the analysis of the TEC responses during the events carried out in this work, we performed a brief statistical analysis on the day-to-day variability of the quiet-time TEC. The objective was to measure the usual day-to-day variability observed for quiet-time TEC in South America in order to verify if the TEC changes were significant during the events analyzed here. We found that the stations Salu and Areq (equatorial) presented a usual quiet-time day-to-day variability of $\sim 7\,\%$. On the other hand, the stations Bogt and Poli (EIA crest) presented quiet-time day-to-day variability of ~ 10–$17\,\%$. The quiet days considered were 7–12 March (related to March event) and 27 July–1 August (related to August event).

3.1 Event of 13–31 March 2013

The first event studied in this work occurred on 13–31 March 2013 during the equinox. Figure 2 shows the solar wind parameters such as the solar wind speed (V_SW), the interplanetary magnetic field B_z component (IMF B_z) and the interplanetary electric field E_y component (IEF E_y). The geomagnetic conditions given by AE, Sym-H and Kp indexes

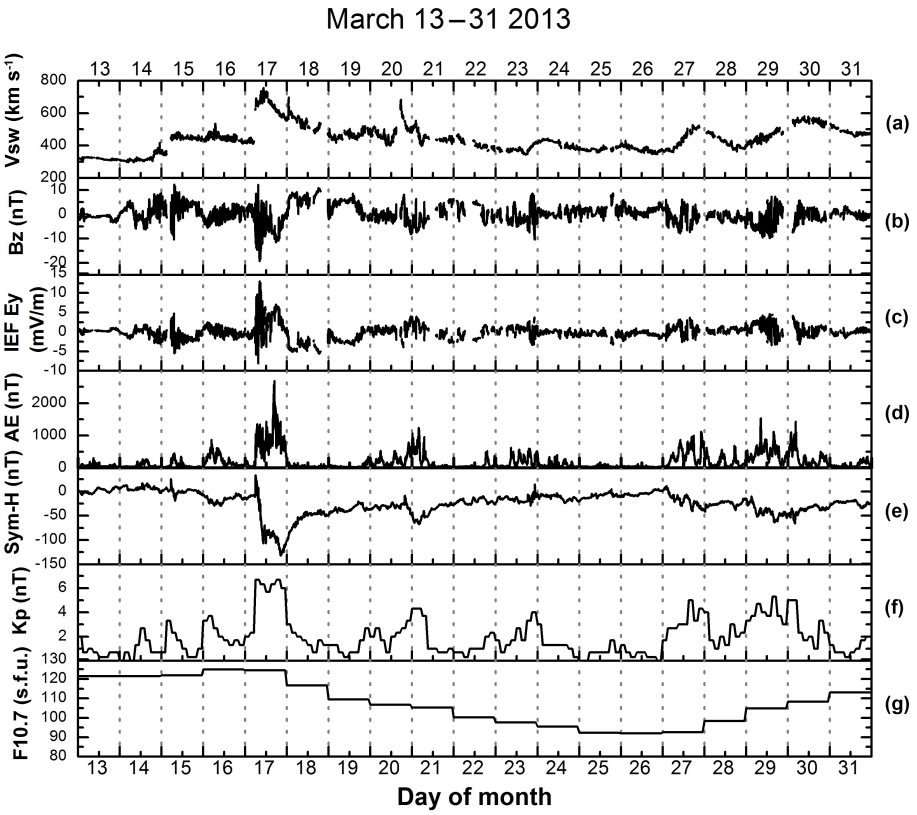

Figure 2. (a–g) Solar wind speed, IMF B_z component, IEF E_y electric field, AE index, Sym-H index, Kp index and F10.7 solar flux for the period 13–31 March 2013.

Table 1. Locations of four GPS stations and two magnetometers used in this work.

Site	Geographic latitude	Geographic longitude	Dip angle	Local time
Arequipa (Areq)	16.46° S	71.49° W	8.94° S	LT = UT−5
São Luís (Salu)	2.60° S	44.21° W	8.73° S	LT = UT −3
Bogota (Bogt)	4.64° N	74.08° W	37.70° N	LT = UT−5
São Paulo (Poli)	23.20° S	45.86° W	37.15° S	LT = UT−3
Jicamarca	11.95° S	76.87° W	0.06° N	LT = UT−5
Piura	5.20° S	80.65° W	12.52° N	LT = UT−5

and the F10.7 solar flux index are also shown in Fig. 2. The quiet-time reference used in this analysis was the 13 March when the Kp index was under 3. Regarding the TEC measurements, the quiet-time reference was taken as the TEC average from the period 7–12 March, which presented no significant disturbances from solar wind and Kp under 3. A less pronounced increase in V_{SW} is observed on 15–16 March and associated with this increase we can observe significant southward incursions of IMF B_z (~ -10 nT) and increases in AE index ($\sim$ 500–800 nT).

The geomagnetic storm started on 17 March, around 06:00 UT. The sudden storm commencement can be verified in the Sym-H increase to about 30 nT. At this time the solar wind speed presents a sharp increase from around 450 to 650 km s^{-1} characterizing the shock at the magnetopause. The main phase of the geomagnetic storm initiated at 06:15 UT and lasted until 20:30 UT on 17 March. This was an intense geomagnetic storm with Sym-H dropping to -132 nT, maximum AE index of 2689 nT and the Kp index reaching 7 on 17 March. After 20:30 UT the recovery phase initiated and lasted around 2–3 days. Following this intense disturbance one can observe in Fig. 2 that smaller disturbances are present on 20–24 March, characterized by AE increases, Sym-H decreases, increased geomagnetic activity given by Kp values around 4 and oscillatory IMF B_z.

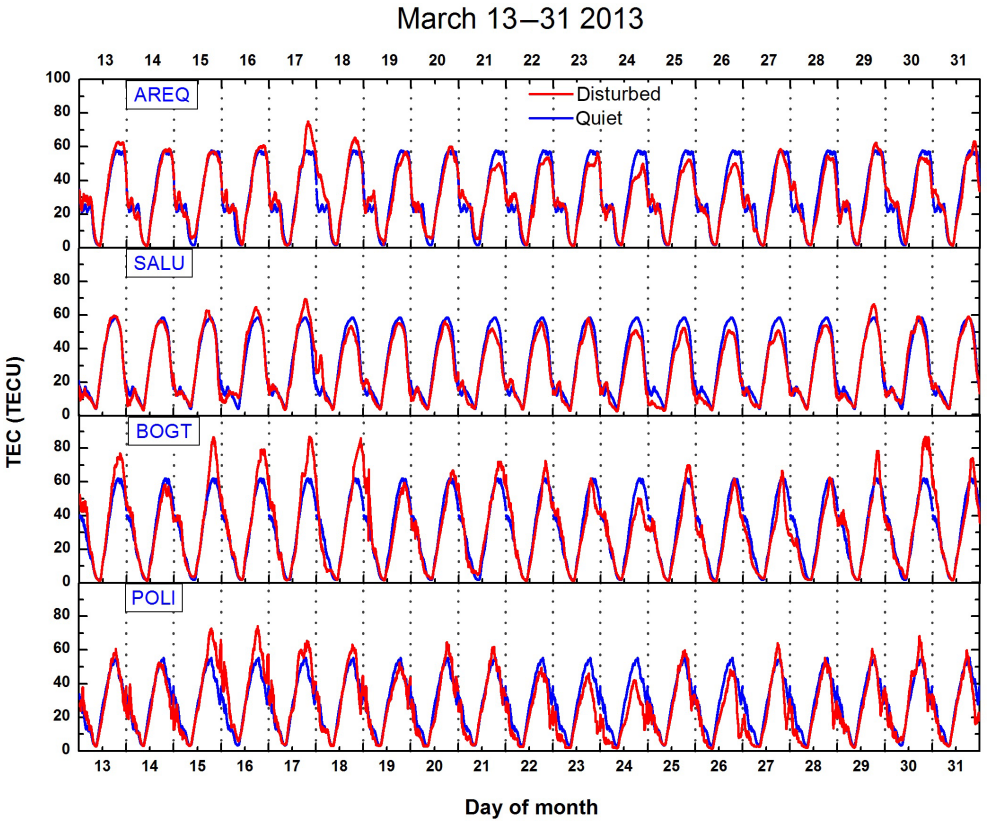

Figure 3. TEC measured over the equatorial GPS stations Areq and Salu, and the EIA crests stations Bogt (north) and Poli (south), for the period 13–31 March 2013. The blue line shows the quiet-time reference values (average of 6 previous quiet days) and the red line shows the disturbed values.

Figure 3 presents the TEC observed for the entire period 13–31 March, over the equatorial GPS stations Areq and Salu and the low-latitude stations Bogt (northern EIA crest) and Poli (southern EIA crest). These TEC curves provide a local view of the TEC behavior during this disturbed period. As stated before, the 6-day period prior to the storm (7–12 March) was taken as quiet-time reference, and the TEC average observed in this period (blue line) was plotted together with the disturbed data (red line) for the entire period. On 15–16 March one can see higher TEC over Poli and Bogt, $\sim 30\,\%$ higher compared to quiet time. On these days, weak but effective disturbances were present, as mentioned before. In this case the action of PPEFs was probably responsible for the TEC enhancements since these are stations located on the EIA crests, which represent a stronger EIA. No TEC responses were observed over the equatorial stations (Areq and Salu) on 15–16 March. On 17 March one can observe TEC enhancements over the four GPS stations analyzed, during the initial and main phases of the geomagnetic storm. The maximum TEC observed on 17 March at each station, compared to quiet time, were 34 % higher over Areq and 19 % higher over Salu (more significant differences than the $\sim 7\,\%$ day-to-day quiet-time variability) as well as 38 % higher over Bogt and 18 % higher over Poli. Around 24:00 UT over Areq and Salu it is possible to observe a peak on the TEC due to the action of a stronger pre-reversal enhancement (PRE). The PRE is an intensification of the $E \times B$ vertical drift during dusk hours over the geomagnetic equator caused by the combination of winds and electric fields around the terminator, and it exhibits dependence with the season and the solar cycle and presents large day-to-day variability (Fejer et al., 1991). The PRE causes the intensification of EIA due to more intense $E \times B$ vertical drift, elevating the F layer to altitudes of lower recombination rates and causing TEC increases during the PRE. This mechanism adds to the PPEF during disturbed times resulting in an even stronger fountain effect and EIA development which is also seen as stronger EIA crests. The TEC enhancements observed on 17 March (main phase of the geomagnetic storm) are comparable to those observed on 15–16 March over Poli and Bogt (prior to the geomagnetic storm). This indicates that those weak disturbances observed on 15–16 March, which are not related to geomagnetic storms, may represent significant effectiveness in TEC responses, in comparison to geomagnetic storms. The F10.7 solar flux remained almost unaltered on 14–17 March and decreased after this period. It is interesting to note that

TEC shows no DD pattern during the recovery phase of the geomagnetic storm (18–19 March).

Moving forward to the period 20–25 March in Fig. 3, one can observe that TEC is slightly lower than the quiet-time reference especially over the equatorial sector (Areq and Salu). Also, on these days weaker solar and geomagnetic disturbances were present as one can see from Fig. 2. Moreover, the F10.7 was decreasing in this period, which is consistent with lower TEC values. No significant neutral composition changes in South America that could create TEC changes were observed during this period of March, as shown by the O / N_2 ratio, seen in Fig. 4. The objective of showing the O / N_2 is to exclude the thermospheric neutral forcing as an effective source of TEC changes in this event.

The HILDCAAs events studied in this work meet at least three of the four criteria proposed by Tsurutani and Gonzalez (1987) which were discussed previously. It is important to make sure that the criteria are being fulfilled in order to distinguish the HILDCAA phenomenon from other physical mechanisms such as the occurrence of substorms (not analyzed here), as discussed by Tsurutani et al. (2006). One important feature examined in both periods analyzed in this work is the correlation between the negative incursions of the IMF B_z and the decreases in Sym-H, which show a direct relationship such as the results presented by Tsurutani et al. (2006). Moreover, for major negative incursions of IMF B_z we can observe a corresponding AE increase. Figure 5 shows the IMF B_z and the geomagnetic indexes AE and Sym-H for the 4 days considered as HILDCAA in this event (27–30 March). Figure 5 was created to show a zoomed-in view of the parameters discussed above. For this period it is clear that the AE index was less active on 28 March, and thus it was not possible to follow all the criteria. On the other hand, as discussed earlier, the criteria adopted to classify a HILDCAA phenomenon were extreme, and in this case we believe that the conditions observed on 27–30 March can provide a satisfactory scenario of the ionospheric responses. The same type of restriction in accomplishing all HILDCAA criteria was found in other studies (Koga et al., 2011). The maximum AE observed in this period was 1535 nT and the average value was 327.39 nT. Sym-H reached around −50 nT in the period. Considering this HILDCAA event, except for 29–30 March, the TEC responses showed in Fig. 3 presented no significant changes. As discussed earlier the solar wind disturbances are less intense on 28 March, which may have caused this weak response for the HILDCAA period. On the other hand, on 30 March the TEC presented a strong increase over Bogt (38 % higher) and Poli (20 % higher), which may be explained as a PPEF action due to the IMF B_z southward incursions and consequently the magnetic reconnection at magnetopause and the input of solar energy at auroral region. However, no significant TEC changes were observed over the equatorial stations. In this case the penetration of the interplanetary electric field (IEF) to the auroral and low-latitude ionosphere at dayside adds to the zonal electric field at the equator and causes a strengthening of EIA. A stronger eastward zonal electric field at the equatorial region causes an increase in the upward vertical plasma drift ($E \times B$ drift) leading the plasma to higher altitudes where the ion recombination rates are lower and consequently the TEC remains higher, as discussed earlier. The stronger EIA crests discussed above are also related to the higher solar flux observed on 27–30 March. However, the F10.7 increase for this period did not produce TEC enhancements over all stations analyzed.

In order to verify the occurrence of PPEFs during the disturbances we present the Jicamarca–Piura ΔH and the IEF E_{rec} data in Fig. 6. Considering the first day of this period (13 March) as the quiet-time reference for the ΔH data, the maximum ΔH observed was 79 nT with no signature of PPEFs. Such signatures are represented by fast and large variations on the ΔH simultaneously with E_{rec}. One can observe from the magnetometer data (black line) that on 14 March less pronounced disturbances are present, which is consistent with the interplanetary electric field (IEF) disturbances (blue line); however, the maximum ΔH is lower than the quiet-time reference. Daytime for Jicamarca–Piura data is from 11:00 to 23:00 UT and the relationship between ΔH and the zonal electric field is valid only for daytime. It is possible to identify periods of high correlation between the ΔH and the IEF E_{rec} which denotes the occurrence of PPEF. Following this methodology, the most prominent PPEF are observed on 14, 17, 20 and 27–29 March. It is worth remarking here that the PPEF adds to the zonal electric field at ionosphere; the shape of both curves (ΔH and IEF E_{rec}) is quite different but it is important to observe the rapid and intense variations of IEF that are being transmitted to the equatorial ionosphere. There is a time delay between the solar wind disturbances and the equatorial response (magnetometer data); from the data presented here this time delay is about 15 min. On 16–17 March it is possible to observe that ΔH is higher than quiet-time reference, which is consistent with higher zonal electric fields and TEC values. On 17 March a strong signature of PPEF can be seen from 12:00 to 17:00 UT.

Despite the PPEF signature being strong on 29 March, the rapid incursions of ΔH (which are directly related to the vertical drifts at the equatorial zone) did not cause strong TEC responses over all stations since the strength of the vertical drifts were not sustained for long enough to cause substantial TEC increases. For this reason the long-lasting PPEFs are more effective in producing TEC enhancements at low-latitude and equatorial regions than the rapid PPEFs (de Siqueira et al., 2011). The ΔH for 30 March is higher than on 13 March, denoting higher zonal electric fields and vertical drifts at the equator, which appears to be the most important forcing for the TEC enhancements observed on 30 March due to the stronger EIA. Except for 30 March, the global response for this HILDCAA event is considered weak compared to the responses observed during the geomagnetic storm, and the likely reason is the weaker solar

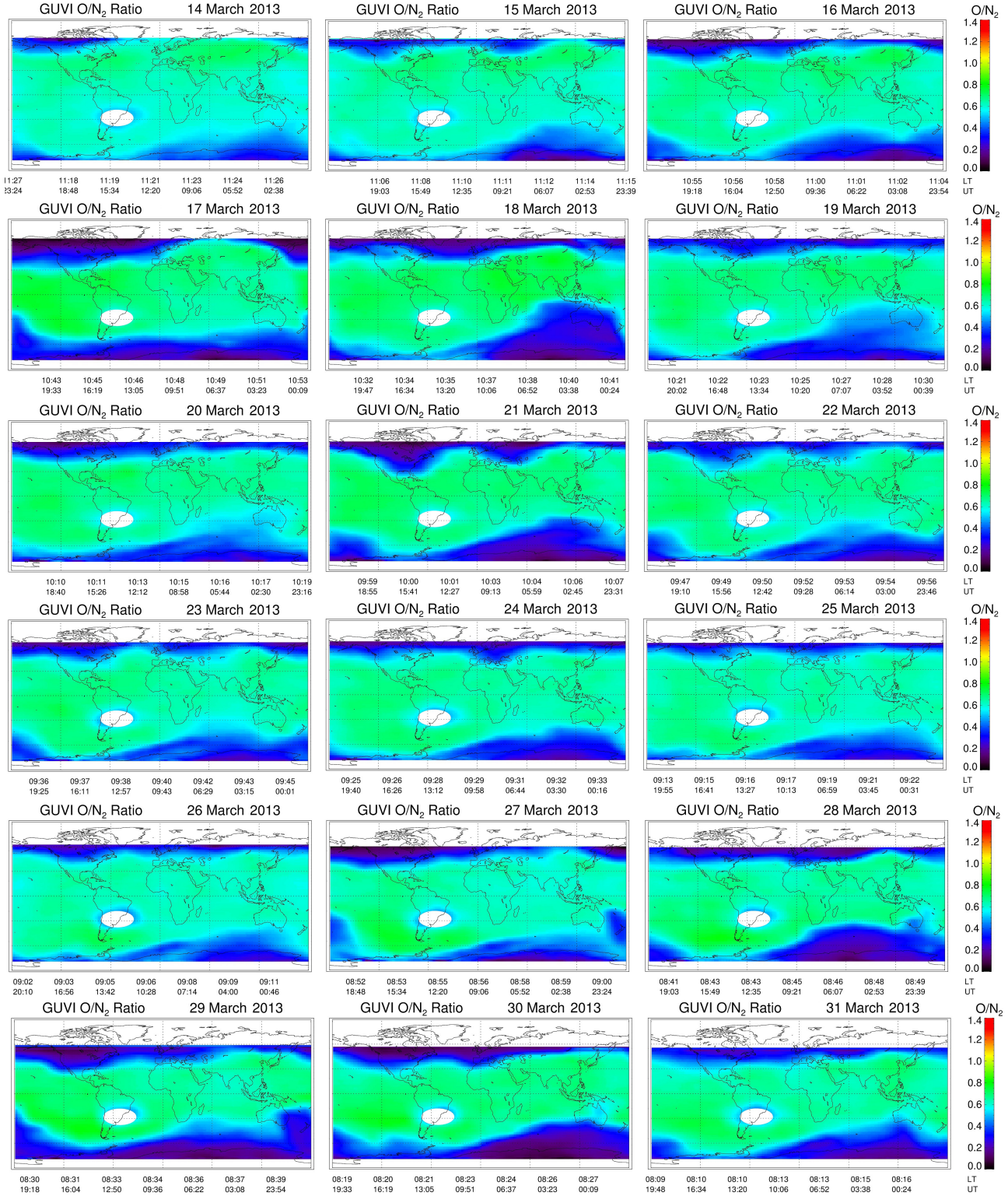

Figure 4. O / N_2 ratios measured by the GUVI instrument onboard the TIMED satellite, for the period 14–31 March 2013.

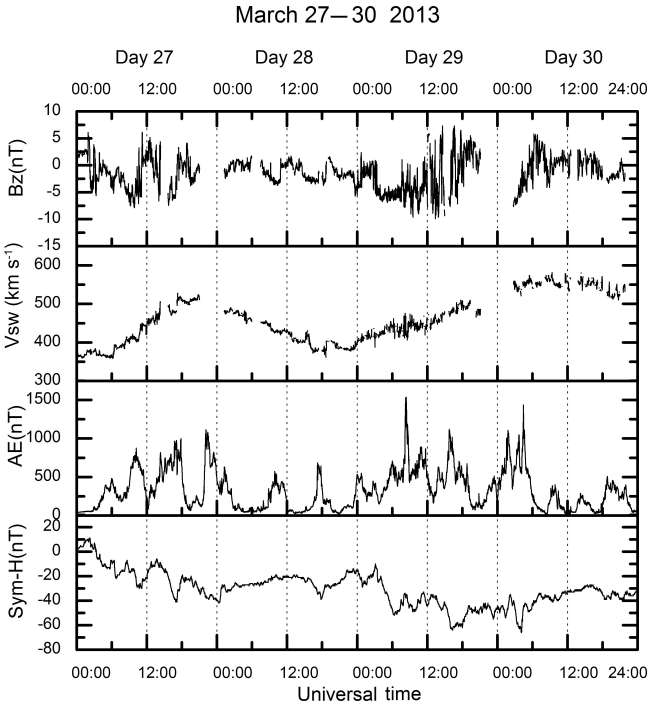

Figure 5. Zoomed-in view of the HILDCAA period which occurred on 27–30 March 2013 showing the IMF B_z component, solar wind speed V_{SW}, AE index and Sym-H index.

forcing on 28 March. On the other hand, this particular event of March gives important information regarding the prompt ionospheric responses to solar forcing. Also, we show that the PPEFs are the most important source of TEC changes during this period, especially considering the modulation of the EIA.

3.2 Event of 2–20 August 2013

The second and most important period analyzed in this work occurred on 2–20 August 2013, during the transition from winter solstice to equinox. Figure 7 presents the solar wind parameters and the geomagnetic indices AE, Kp and Sym-H. The F10.7 solar flux is presented in the bottom panel. The first day of this period was considered as the quiet-time reference with no external disturbances and Kp value around 1. Regarding the TEC measurements, the quiet-time reference was taken as the TEC average of the period 27 July to 1 August, which presented no significant disturbances from solar wind and Kp under 3. The geomagnetic storm initiated on 4 August around 15:00 UT, when one can observe a sudden increase in the solar wind speed from ~ 350 to $\sim 600\,\mathrm{km\,s^{-1}}$. The main phase lasted until 02:20 UT on 5 August, when the recovery phase initiated. The minimum Sym-H measured in the period was -56 nT, i.e., a moderate geomagnetic storm. The recovery phase lasted around 4 days. Following the geomagnetic storm, it is clear from Fig. 7 that disturbances are present on days 9–10 August characterized by oscillatory IMF B_z and a faster solar wind structure impinging magnetopause. However, this faster solar wind of about $\sim 500\,\mathrm{km\,s^{-1}}$ on 9 August was not responsible for creating a disturbed geomagnetic scenario as showed by Kp, AE and Sym-H indices. Moving forward to 13–17 August, it is possible to observe that solar wind and geomagnetic disturbances are present, characterized by AE increases, Sym-H decreases, increased geomagnetic activity given by Kp values around 4–5 and oscillatory IMF B_z. Then, the HILDCAA event considered in this period occurred from 15 to 17 August, based on the analysis of the criteria discussed earlier.

The local ionospheric response can be seen from TEC data in Fig. 8. The quiet-time reference data (average of quiet days; blue line) is plotted together with the disturbed data (red line). The geomagnetic storm response is noticed to be slightly higher TEC over Areq, Bogt and Poli on 4 August (main phase) compared to quiet-time reference; however, these enhancements are not stronger than the usual quiet-time variability. Poli and Bogt present prominent TEC enhancements related to the PRE, at the end of 4 August, which denotes a stronger EIA. Salu showed no response during the main phase of the geomagnetic storm. During the recovery phase on 5 August, Salu and Bogt presented lower TEC values compared to quiet-time reference, in spite of TEC over Areq and Poli remaining slightly higher. Only Bogt (northern EIA crest) presents a strong negative phase of the ionospheric storm, showing lower TEC. No outstanding responses were observed in TEC during this moderate geomagnetic storm. Considering the seasonal period, a moderate response was expected, as observed. In the period 8–13 August, TEC showed enhancements over the EIA crests, while geomagnetic activity and F10.7 presented no significant changes. In order to confirm the occurrence of PPEF for the whole period, we show in Fig. 9 the magnetometer ΔH data plotted with the IEF E_{rec} data during the disturbed period. Taking the first day of this period (2 August) as the quiet-time reference for ΔH observations and comparing the blue and black lines of Fig. 9, it is possible to observe that the period 8–13 August presents ΔH changes, such as PPEF and increased magnitude, which are directly related to changes in zonal electric fields/vertical drifts at the equator as discussed earlier, leading to EIA development modifications. It is clear in Fig. 9 that the most effective PPEF occurred on 4, 5, 13, 15 and 16 August, i.e., during the main phase of the geomagnetic storm and during the HILDCAA event, except for 13 August, which presents solar wind disturbances (southward IMF B_z incursions) and moderate geomagnetic activity, but this is prior to the HILDCAA event. PPEFs are also observed on 5, 14, 17–19 August, which shows that this electrodynamic scenario may prevail for several days and is highly governed by the external solar wind forcing.

The most striking point here is the ionospheric response during the HILDCAA period from 15 to 17 August. Even on 14 August observed higher TEC is observed over all stations

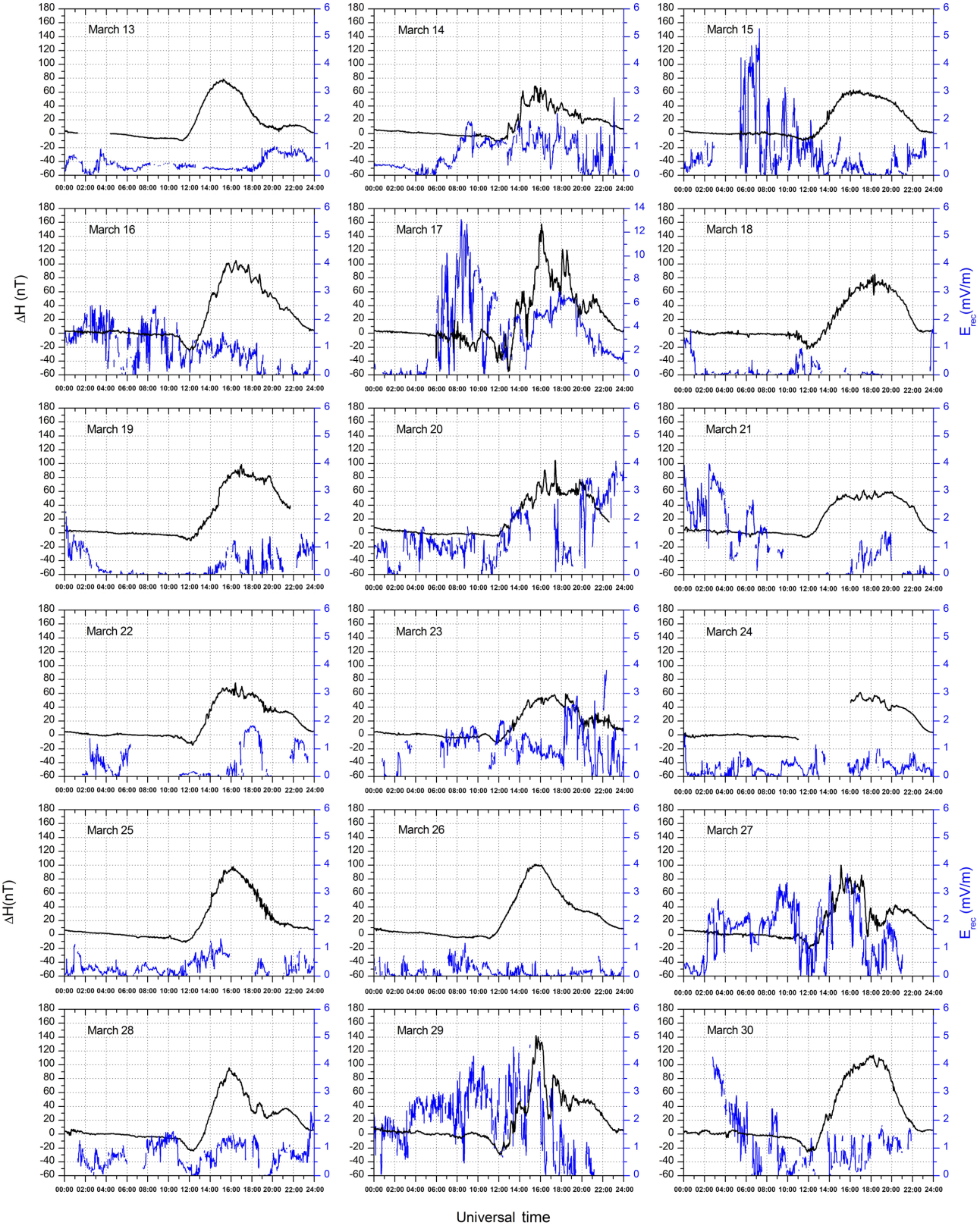

Figure 6. ΔH Jicamarca–Piura (black line) and IEF E_{rec} (blue line) from 13 to 30 March, showing the occurrence of PPEF.

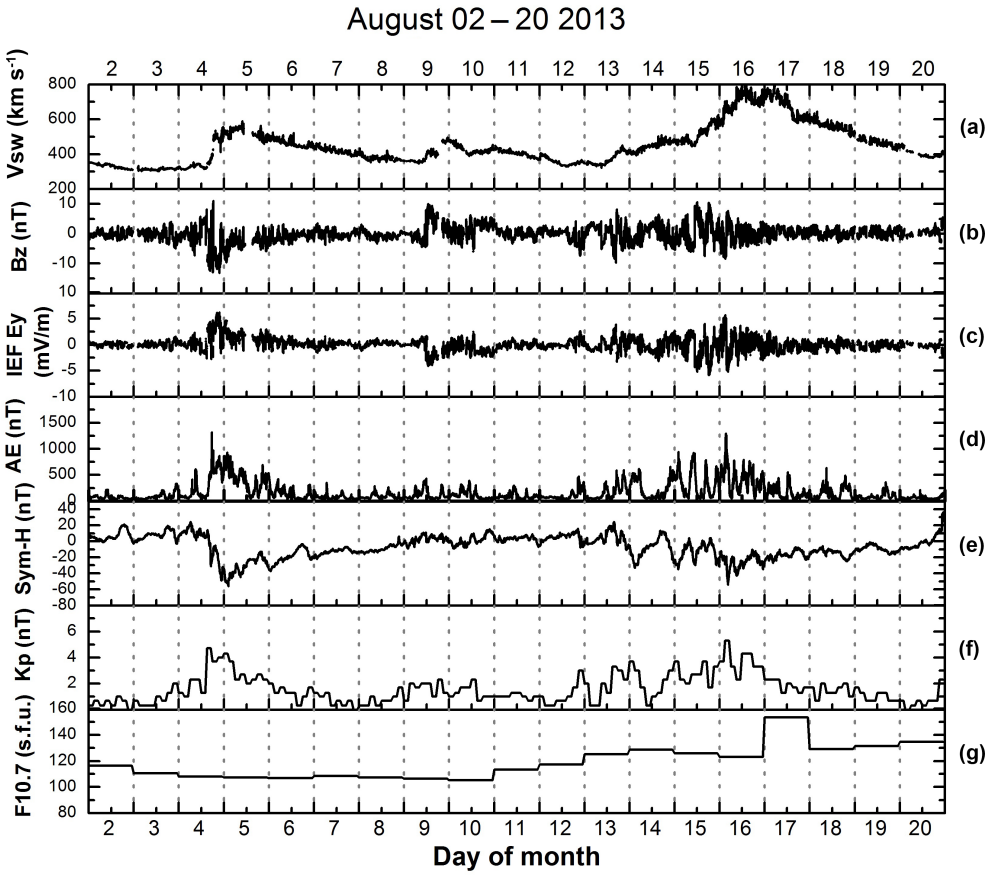

Figure 7. (a–g) Solar wind speed, IMF B_z component, IEF E_y electric field, AE index, Sym-H index, Kp index and F10.7 solar flux for the period 2–20 August 2013.

and the most pronounced enhancement was measured over Poli. The southward incursions of the IMF B_z component and AE index increases noticed on 13–14 August were responsible for creating this disturbed scenario right before the actual HILDCAA event (15–17 August). Also, the IMF B_z and IEF E_y oscillated for a longer time during the HILDCAA compared to the geomagnetic storm, establishing the continuous and effective scenario for the ionospheric responses. The F10.7 shows an enhancement of $\sim$ 110 s.f.u. on 9 August to $\sim$ 130 s.f.u. on 14 August and remained at this level, except for 17 August, which showed an increase to $\sim$ 150 s.f.u. However, TEC showed enhancements prior to 17 August and also after this day. Therefore, this particular F10.7 enhancement is not the main source of the TEC responses observed in the whole HILDCAA event. This disturbed scenario continues up to 20 August when the solar wind parameters and the geomagnetic indexes returned to a quiet pattern. Thus, the HILDCAA event in this period was responsible for generating a strong ionospheric response at equatorial and low-latitude regions.

Table 2 presents the percent deviations from the quiet-time reference observed in TEC during this HILDCAA event, showing that the TEC was intensified during the whole event, exhibiting enhancements much higher than the quiet-time variability discussed on Sect. 3.

Table 2. Percent deviations (enhancements) observed in disturbed TEC compared to quiet-time reference (August event) by station.

Date	Areq	Salu	Bogt	Poli
14 Aug	15 %	–	33 %	65 %
15 Aug	23 %	–	43 %	55 %
16 Aug	26 %	22 %	46 %	82 %
17 Aug	26 %	17 %	38 %	58 %
18 Aug	23 %	17 %	33 %	75 %
19 Aug	15 %	15 %	43 %	34 %
20 Aug	17 %	17 %	36 %	38 %

The TEC values observed during this HILDCAA period were much higher than the values observed during its precedent moderate geomagnetic storm, as shown in Table 2. It is also clear that the southern station Poli responded more effectively to the disturbances than the northern station Bogt. This asymmetry observed in the EIA crests is often attributed to meridional winds (Balan et al., 1997). Based on these results,

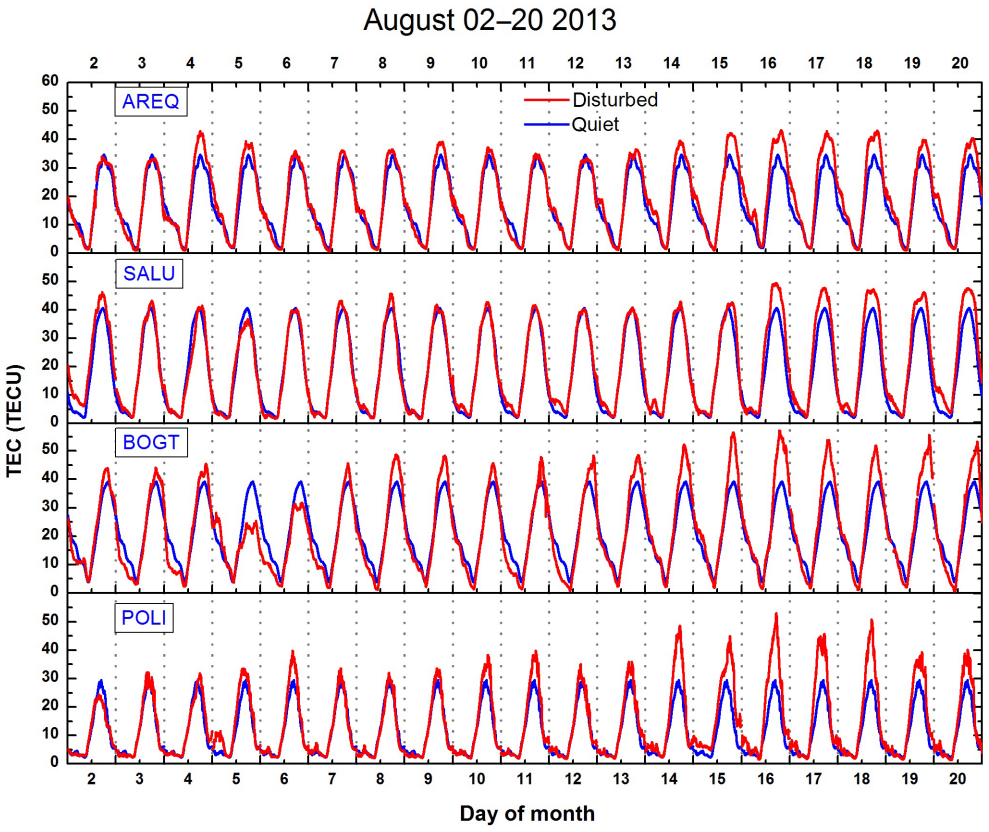

Figure 8. TEC measured over the equatorial GPS stations Areq and Salu, and the EIA crests stations Bogt (north) and Poli (south), for the period 2–20 August 2013. The blue line shows the quiet-time reference (average of 6 previous quiet days) and the red line shows the disturbed values.

a HILDCAA event may be more effective for ionospheric response in comparison to moderate geomagnetic storms, considering the seasonal conditions. This conclusion is of the most importance if we consider the ionospheric models in use currently, regarding the input parameters. In this period, Sym-H index presents comparable negative values during the geomagnetic storm and the HILDCAA event but the TEC observations show completely different ionospheric responses for both phenomena. Such differences become a challenge for modelers and require more study and statistics involving these phenomena.

The TEC enhancements shown in Fig. 8 were likely caused by the action of PPEFs due to the oscillatory behavior of IMF B_z during the HILDCAA event. Verkhoglyadova et al. (2011) showed the role of PPEFs and DD as the main source of VTEC (vertical TEC) changes during (CIR-associated) HILDCAAs related directly to the continuous solar wind forcing. Another factor that probably contributed to such enhancements is the increase observed in F10.7 solar flux (Fig. 7) which enhances the atmospheric ionization. In order to verify the neutral composition changes for this period, the O / N_2 ratios retrieved by the GUVI instrument are presented in Fig. 10. There is a lack of data from 6 to 14 August, but the data available are useful to provide the neutral scenario during the geomagnetic storm and the HILDCAA event. Based on O / N_2 data, it is possible to observe that during the HILDCAA event, the ratios were lower than during the previous geomagnetic storm. Lower O / N_2 ratios are related to decreases in ionospheric ionization and consequently TEC decreases. However, we observe higher TEC during the HILDCAA event. Then there is no relationship between neutral composition changes and the TEC enhancements observed during this HILDCAA event. This type of anti-correlation between the O / N_2 ratio and the disturbed TEC was also reported by Mannucci et al. (2009). The only objective of showing the O / N_2 ratio of this period was to exclude the neutral composition forcing as a source of TEC changes during this event. Our main objective is to emphasize the PPEFs and solar wind forcing as main sources of TEC changes during the HILDCAA event. Based on the TEC responses observed in this August event, one can observe a weak ionospheric response for the geomagnetic storm whereas the ionospheric response for the HILDCAA event is much stronger. In this case it is imperative to consider the seasonal conditions since one can expect lower TEC during this winter-to-equinox period. On the other hand the effec-

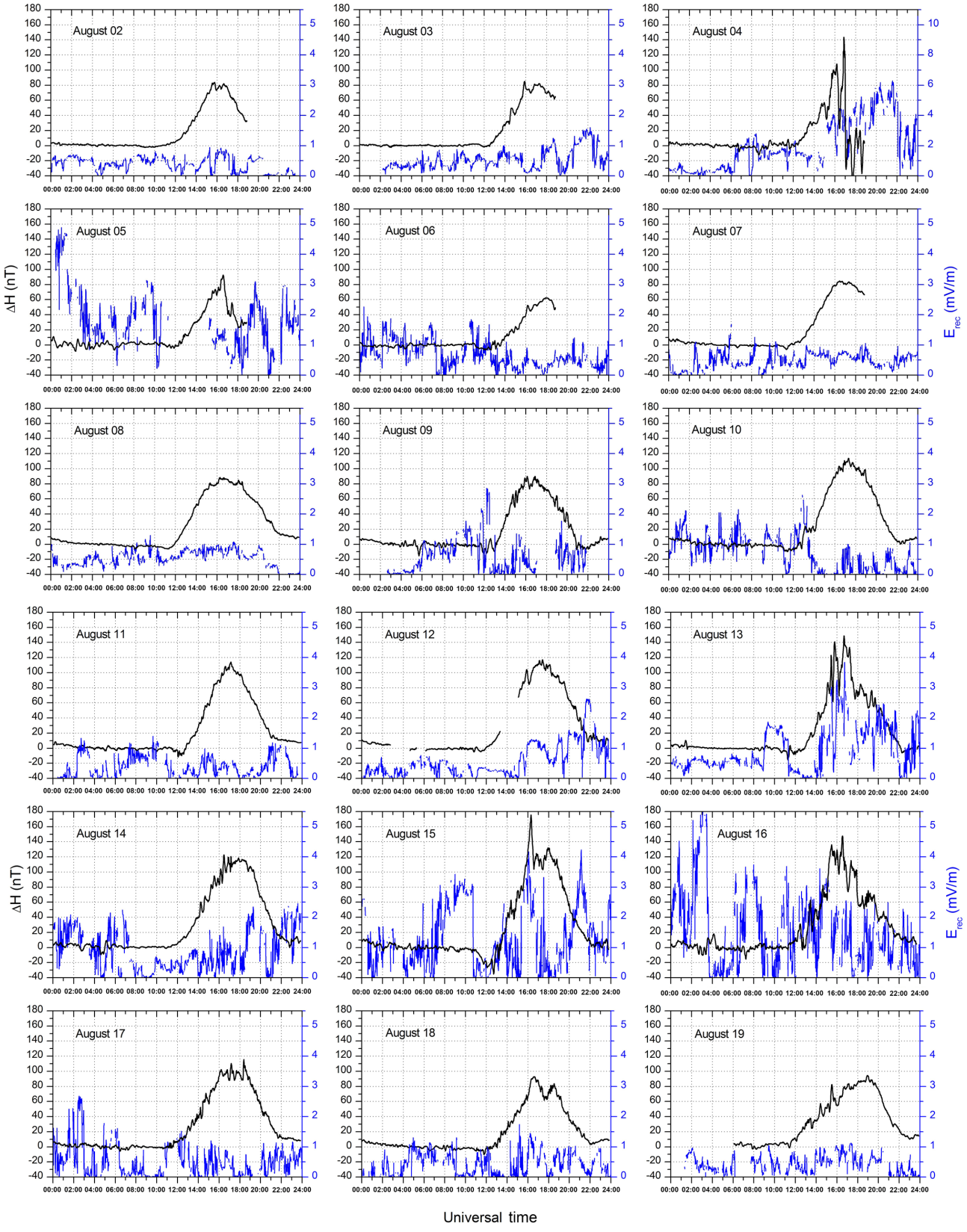

Figure 9. ΔH Jicamarca–Piura (black line) and IEF E_{rec} (blue line) from 2 to 19 August, showing the occurrence of PPEF.

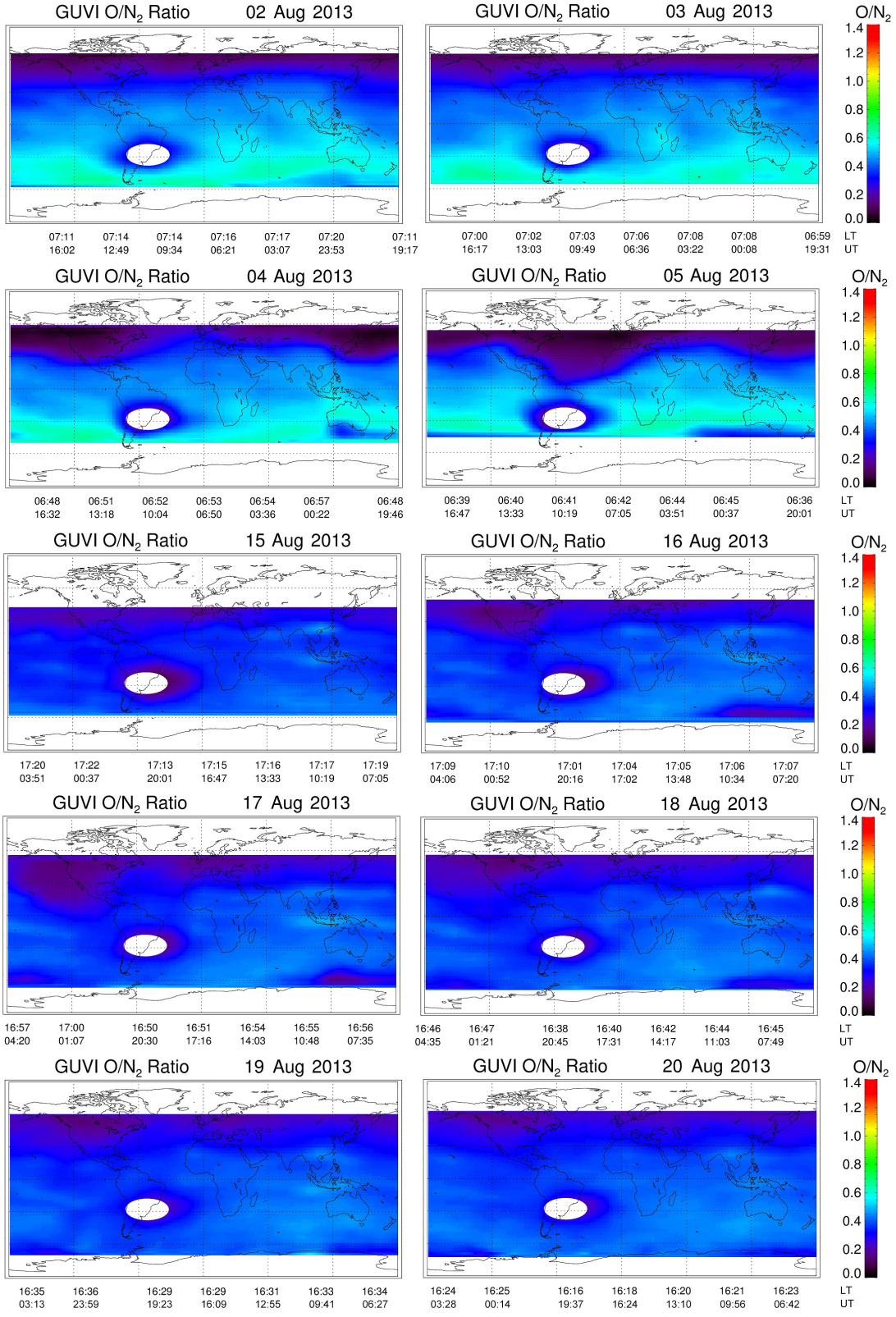

Figure 10. O / N_2 ratios measured by the GUVI instrument onboard the TIMED satellite, for the period 2–5 and 15–20 August 2013.

tiveness of the HILDCAA event in generating TEC enhancements for this period is striking.

4 Conclusions

In this work we aimed to demonstrate the ionospheric sensibility related to solar wind forcing by means of TEC measurements. The solar wind conditions and ionospheric responses observed in TEC and magnetometer data at the equatorial region have been shown and analyzed in order to provide information on the effectiveness of HILDCAA events for such responses. GUVI O / N_2 ratios were analyzed in order to verify their relationship to TEC changes. Different ionospheric responses were observed considering two periods of 2013: March and August. These periods were carefully selected due to the occurrence of a geomagnetic storm followed by a HILDCAA event, which was observed in both periods. Then it was feasible to compare them and show the differences of the ionospheric behavior. For the March period, the main features were an intense geomagnetic storm followed by a 3-day HILDCAA event (with strong AE increases), and the ionospheric responses can be summarized as follows: intense response for the geomagnetic storm and weak response for the HILDCAA event. However, the March HILDCAA is weaker due to the decrease in solar wind forcing on 28 March, and this is the main cause for this weaker HILDCAA response in March. For the August period the main features were a moderate geomagnetic storm followed by a 4-day HILDCAA event (with AE peaks of less intensity compared to the March event), and the ionospheric responses can be summarized as follows: no significant TEC enhancements for the geomagnetic storm and intense TEC increases for the HILDCAA event. In this second period particularly it is important to mention that Sym-H index reached comparable values during the geomagnetic storm and the HILDCAA event, but the HILDCAA was much more effective for the ionospheric response. The TEC increases observed in this August HILDCAA event were not related to neutral composition changes, and the most important forcing was external solar wind and simultaneous/long-duration PPEFs. The TEC exhibited enhancements from 25 to 80 % during the August HILDCAA. These enhancements were much higher than those observed during the previous magnetic storm, and were also much higher than the TEC observed in the days before the HILDCAA event. This is the main point of this work: examining the great effectiveness of a HILDCAA event in generating ionospheric responses. The other main objective of this work was to emphasize the PPEFs and solar wind forcing as main sources of TEC changes during the HILDCAA events analyzed here. As mentioned previously, such differences become a challenge for modelers and require more study and statistics involving these phenomena. The PPEFs during HILDCAA events play an important role regarding ionospheric responses as TEC enhancements. The well-known responses regarding geomagnetic storms, such as higher TEC during the main phase of the storm and lower TEC during the recovery phase (DD action), were observed. This work provided an opportunity to observe the ionospheric responses over (equatorial and low-latitude) South America for two geomagnetic storms and two HILDCAA events and to compare the results since these phenomena were consecutive. Thus, the completely different ionospheric responses to solar wind forcing have been shown and require further investigation in order to be considered properly in ionospheric models for space weather predictions. Finally, it is worth pointing out that long-duration events such as HILDCAAs can affect the low-latitude ionosphere in very distinct ways, especially due to many variable conditions during which they occur. Further studies are in progress to improve the understanding of their influence on the Brazilian low-latitude ionosphere.

Data availability. The geomagnetic data and the F10.7 index used in this work were obtained from the low-resolution OMNIWeb database (http://omniweb.gsfc.nasa.gov/form/dx1.html). The solar wind plasma and interplanetary magnetic field parameters measured by the ACE satellite were obtained from the high-resolution OMNIWeb database (http://omniweb.gsfc.nasa.gov/form/omni_min.html). The Jicamarca–Piura magnetometer data were retrieved from the Jicamarca Radio Observatory at http://jro.igp.gob.pe/database/magnetometer/html/magdata.htm. The GPS data from International GNSS System (IGS) stations located in South America were downloaded from the Scripps Orbit and Permanent Array Center (SOPAC) Garner GPS archive at http://garner.ucsd.edu. The Brazilian data were retrieved from the Brazilian Network for Permanent Monitoring (RBMC) of the Brazilian Institute of Geography and Statistics (IBGE) at http://www.ibge.gov.br/home/geociencias/download/tela_inicial.php?tipo=8. The Global Ultraviolet Imager (GUVI) data were retrieved from http://guvitimed.jhuapl.edu.

Competing interests. The authors declare that they have no conflict of interest.

Special issue statement. This article is part of the special issue "Space weather connections to near-Earth space and the atmosphere". It is a result of the 6° Simpósio Brasileiro de Geofísica Espacial e Aeronomia (SBGEA), Jataí, Brazil, 26–30 September 2016.

Acknowledgements. The authors are thankful to Fundação de Amparo à Pesquisa do Estado de São Paulo (FAPESP) for the partial financial support through process 2012/06949-0 and to Coordenação de Aperfeiçoamento de Pessoal de Nível Superior (CAPES) through Programa Nacional de Pós Doutorado. We are thankful to the Jicamarca Radio Observatory for providing the magnetometer data. The Jicamarca Radio Observatory is a facility of the Instituto Geofisico del Peru and is operated with support from the NSF Cooperative

Agreement ATM-0432565 through Cornell University. Eurico Rodrigues de Paula acknowledges the support of Conselho Nacional de Desenvolvimento Científico e Tecnológico (CNPq), through grant 310802/2015-6. Claudia Maria Nicoli Candido thanks CNPq for the financial support through the process 400373/2014-9. The authors are thankful to Instituto Brasileiro de Geografia e Estatística (IBGE/Brazil) and IGS for providing the GNSS data. We are also thankful to Cesar Valladares for providing the TEC calculation code used in this work.

The topical editor, Ana G. Elias, thanks two anonymous referees for help in evaluating this paper.

References

Abdu, M. A., Walker, G. O., Reddy, B. M., de Paula, E. R., Sobral, J. H. A., Fejer, B. G., and Szuszczewicz, E. P.: Global scale equatorial ionization anomaly (EIA) response to magnetospheric disturbances based on the May–June 1987 SUNDIAL-coordinated observations, Ann. Geophys., 11, 585–594, 1993.

Anderson, D., Anghel, A., Yumoto, K., Ishitsuka, M., and Kudeki, E.: Estimating daytime vertical $EtimesB$ drift velocities in the equatorial F-region using ground-based magnetometer observations, Geophys. Res. Lett., 29, 1–4, https://doi.org/10.1029/2001GL014562, 2002.

Anderson, D., Anghel, A., Chau, J., and Veliz, O.: Daytime vertical $E \times B$ drift velocities inferred from ground based magnetometer observations at low latitudes, Adv. Space Res., 2, S11001, https://doi.org/10.1029/2004SW000095, 2004.

Balan, N., Batista, I. S., Abdu, M. A., MacDougall, J., and Bailey, G. J.: Physical mechanism and statistics of occurrence of an additional layer in the equatorial ionosphere, J. Geophys. Res., 103, 169–29,181, https://doi.org/10.1029/98JA02823, 1998.

Blanc, M.: Magnetospheric convection effects at mid-latitudes, 1. Saint-Santin observations, J. Geophys. Res., 88, 211–213, 1983.

Blanc, M. and Richmond, A. D.: The ionospheric disturbance dynamo, J. Geophys. Res., 85, 1669–1686, 1980.

Burton, R. K., McPherron, R. L., and Russell, C. T.: An empirical relationship between interplanetary conditions and Dst, J. Geophys. Res., 80, 4204, https://doi.org/10.1029/JA080i031p04204, 1975.

de Siqueira, P. M., de Paula, E. R., Muella, M. T. A. H., Rezende, L. F. C., Abdu, M. A., and Gonzalez, W. D.: Storm-time total electron content and its response to penetration electric fields over South America, Ann. Geophys., 29, 1765–1768, https://doi.org/10.5194/angeo-29-1765-2011, 2011.

Fejer, B. G.: Equatorial ionospheric electric fields associated with magnetospheric disturbances, in: Solar Wind-Magnetosphere Coupling, edited by: Kamide, Y. and Slavin, J. A., Terra Sci., Tokyo, 519– 545, 1986.

Fejer, B. G.: The electrodynamics of the low-latitude ionosphere: Recent results and future challenges, J. Atmos. Sol.-Terr. Phys., 59, 1465–1482, 1997.

Fejer, B. G. and Scherliess, L.: Empirical models of storm time equatorial electric fields, J. Geophys. Res., 102, 24047, https://doi.org/10.1029/97JA02164, 1997.

Fejer, B. G., de Paula, E. R., Gonzalez, S. A., and Woodman, R. F.: Average vertical and zonal F-region plasma drifts over Jicamarca, J. Geophys. Res., 96, 13901–13906, 1991.

Foster, J. and Rich, F.: Prompt midlatitude electric field effects during severe geomagnetic storms, J. Geophys. Res., 103, 26367–26372, https://doi.org/10.1029/97JA03057, 1998.

Fuller-Rowell, T. J., Codrescu, M. V., Roble, R. G., and Richmond, A. D.: How does the thermosphere and ionosphere react to a geomagnetic storm?, in: Magnetic Storms, Geophysical Monograph Series, edited by: Tsurutani, B. T., Gonzalez, W. D., Kamide, Y., and Arballo, J. K., AGU, Washington, DC, Vol. 98, https://doi.org/10.1029/GM098p0203, 1997.

Gonzales, C. A., Kelley, M. C., Fejer, B. G., Vickrey, J. F., and Woodman, R. F.: Equatorial electric fieds during magnetically disturbed conditions, II. Implications of simultaneous auroral and equatorial measurements, J. Geophys. Res., 84, 5803–5812, 1979.

Gonzalez, W. D., Joselyn, J. A., Kamide, Y., Kroehl, H. W., Rostoker, G., Tsurutani, B. T., and Vasyliunas, V. M.: What is a geomagnetic storm?, J. Geophys. Res., 99, 5771–5792, https://doi.org/10.1029/93JA02867, 1994.

Heelis, R. A. and Coley, W. R.: East-west ion drifts at mid-latitudes observed by Dynamics Explorer 2, J. Geophys. Res., 97, 19461–19469, 1992.

Huang, C.-S., Foster, J. C., Yumoto, K., Chau, J. L., and Veliz, O.: Prompt effects of solar wind variations on the inner magnetosphere and midlatitude ionosphere, Adv. Space Res., 36, 2407–2412, https://doi.org/10.1016/j.asr.2003.09.069, 2005a.

Huang, C.-S., Foster, J. C., and Kelley, M. C.: Long-duration penetration of the interplanetary electric field to the low-latitude ionosphere during the main phase of magnetic storms, J. Geophys. Res., 110, A11309, https://doi.org/10.1029/2005JA011202, 2005b.

Huba, J. D., Joyce, G., Sazykin, S., Wolf, R., and Spiro, R.: Simulation study of penetration electric field effects on the low- to mid-latitude ionosphere, Geophys. Res. Lett., 32, L23101, https://doi.org/10.1029/2005GL024162, 2005.

Kelley, M. C., Fejer, B. G., and Gonzales, C. A.: An explanation for anomalous ionospheric electric fields associated with a northward turning of the interplanetary magnetic field, Geophys. Res. Lett., 6, 301–304, 1979.

Kelley, M. C., Makela, J. J., Chau, J. L., and Nicolls, M. J.: Penetration of the solar wind electric field into the magnetosphere/ionosphere system, Geophys. Res. Lett., 30, 1158, https://doi.org/10.1029/2002GL016321, 2003.

Kelley, M. C., Ilma, R. R., Nicolls, M., Erickson, P., Goncharenko, L., Chau, J. L., Aponte, N., and Kozyra, J. U.: Spectacular low- and mid-latitude electrical fields and neutral winds during a superstorm, J. Atmos. Sol.-Terr. Phys., 72, 285–291, https://doi.org/10.1016/j.jastp.2008.12.006, 2010.

Klobuchar, J. A.: Ionospheric Effects on GPS, in: Global Positioning System: Theory and Applications, Vol 2, edited by: Parkinson, B. W. and Spilker, J. J., Progress in Astronautics and Aeronautics, Vol. 164, p. 485, 1996.

Koga, D., Sobral, J. H. A., Gonzalez, W. D., Arruda, D. C. S., Abdu, M. A., de Castilho, V. M., Mascarenhas, M., Gonzalez, A. C., Tsurutani, B. T., Denardini, C. M., and Zamlutti, C. J.: Electrodynamic coupling processes between the magnetosphere and the equatorial ionosphere during a 5-day HILDCAA event, J. Atmos. Solar-Terr. Phys., 73, 148–155, https://doi.org/10.1016/j.jastp.2010.09.002, 2011.

Lin, C. H., Richmond, A. D., Heelis, R. A., Bailey, G. J., Lu, G., Liu, J. Y., Yeh, H. C., and Su, S.-Y.: Theoretical study of the low- and midlatitude ionospheric electron density enhancement during the October 2003 superstorm: Relative importance of the neutral wind and the electric field, J. Geophys. Res., 110, A12312, https://doi.org/10.1029/2005JA011304, 2005.

Mannucci, A. J., Tsurutani, B. T., Iijima, B. A., Komjathy, A., Saito, A., Gonzalez, W. D., Guarnieri, F. L., Kozyra, J. U., and Skoug, R.: Dayside global ionospheric response to the major interplanetary events of 29–30 October 2003 "Halloween Storms", Geophys. Res. Lett., 32, L12S02, https://doi.org/10.1029/2004GL021467, 2005.

Mannucci, A. J., Tsurutani, B. T., Abdu, M. A., Gonzalez, W. D., Komjathy, A., Echer, E., Iijima, B. A., Crowley, G., and Anderson, D.: Superposed epoch analysis of the dayside ionospheric response to four intense geomagnetic storms, J. Geophys. Res., 113, A00A02, https://doi.org/10.1029/2007JA012732, 2008.

Mannucci, A. J., Tsurutani, B. T., Kelley, M. C., Iijima, B. A., and Komjathy, A.: Local time dependence of the prompt ionospheric response for the 7, 9, and 10 November 2004 superstorms, J. Geophys. Res., 114, A10308, https://doi.org/10.1029/2009JA014043, 2009.

Mlynczak, M. G., Hunt, L. A., Marshall, B. T., Martin-Torres, F. J., Mertens, C. J., Russell III, J. M., Remsberg, E. E., Lopez-Puertas, M., Picard, R., Winick, J., Wintersteiner, P., Thompson, R. E., and Gordley, L. L.: Observations of infrared radiative cooling in the thermosphere on daily to multiyear timescales from the TIMED/SABER instrument, J. Geophys. Res., 115, A03309, https://doi.org/10.1029/2009JA014713, 2010.

Nishida, A.: Coherence of geomagnetic DP 2 fluctuations with interplanetary magnetic variations, J. Geophys. Res., 73, 5549–5559, 1968.

Prölss, G. W.: Ionospheric F-region storms, in: Handbook of Atmospheric Electrodynamics, edited by: Volland, H., CRC Press, Boca Raton, Vol. 2, 195–248, 1995.

Rastogi, R. G. and Klobuchar, J. A.: Ionospheric electron content within the equatorial F2 layer anomaly belt, J. Geophys. Res., 95, 19045–19052, https://doi.org/10.1029/JA095iA11p19045, 1990.

Reddy, C. A., Somayajulu, V. V., and Devasia, C. V.: Global scale electrodynamic coupling of the auroral and equatorial dynamo regions, J. Atmos.-Terr. Phys., 41, 189–201, https://doi.org/10.1016/0021-9169(79)90012-6, 1979.

Rishbeth, H.: F-region storms and thermospheric circulation, J. Atmos.-Terr. Phys., 37, 1055–1064, 1975.

Sardón, E. and Zarraoa, N.: Estimation of total electron content using GPS data: How stable are the differential satellite and receiver instrumental biases?, Radio Sci., 32, 1899–1910, https://doi.org/10.1029/97RS01457, 1997.

Scherliess, L. and Fejer, B. G.: Storm time dependence of equatorial disturbance dynamo zonal electric fields, J. Geophys. Res., 102, 24037–24046, 1997.

Seemala, G. K. and Valladares, C. E.: Statistics of total electron content depletions observed over the South American continent for the year 2008, Radio Sci., 46, RS5019, https://doi.org/10.1029/2011RS004722, 2011.

Sobral, J. H. A., Abdu, M. A., Gonzalez, W. D., Gonzalez, A. C., Tsurutani, B. T., da Silva, R. R. L., Barbosa, I. G., Arruda, Denardini, C. M., Zamlutti, C. J., and Guarnieri, F.: Equatorial ionospheric responses to high-intensity long-duration auroral electrojet activity (HILDCAA), J. Geophys. Res., 111, A07S02, https://doi.org/10.1029/2005JA011393, 2006.

Tsurutani, B. T. and Gonzalez, W. D.: The cause of high-intensity long-duration continuous AE activity (HILDCAAs): interplanetary Alfven wave trains, Planet. Space Sci., 35, 405–412, 1987.

Tsurutani, B. T., Gonzalez, W. D., Gonzalez, A. L. C., Tang, F., Arballo, J. K., and Okada, M.: Interplanetary origin of geomagnetic activity in the declining phase of solar cycle, J. Geophys. Res., 100, 21717–21733, 1995.

Tsurutani, B. T., Manucci, A., Iijima, B., Abdu, M. A., Sobral, J. H. A., Gonzalez, W., Guarnieri, F., Tsuda, T., Saito, A., Yumoto, K., Fejer, B. G., Fuller-Rowell,T. J., Kozyra, J., Foster, J. C., Coster, A., and Vasyliunas, V. M.: Global dayside ionosphere uplift and enhancement associated with interplanetary electric fields, J. Geophys. Res., 109, A08302, https://doi.org/10.1029/2003JA010342, 2004a.

Tsurutani, B. T., Gonzalez, W. D., Guarnieri, F., Kamide, Y., Zhou, X., and Arballo, J. K.: Are high-intensity long-duration continuous AE activity (HILDCAA) events substorm expansion events?, J. Atmos.-Terr. Phys., 66, 167–176, https://doi.org/10.1016/j.jastp.2003.08.015, 2004b.

Tsurutani, B. T., Gonzalez, W. D., Gonzalez, A. L. C., Guarnieri, F. L., Gopalswamy, N., Grande, M., Kamide, Y., Kasahara, Y., Lu, G., Mann, I., McPherron, R., Soraas, F., and Vasyliunas, V.: Corotating solar wind streams and recurrent geomagnetic activity: A review, J. Geophys. Res., 111, A07S01, https://doi.org/10.1029/2005JA011273, 2006.

Tsurutani, B. T., Verkhoglyadova, O. P., Mannucci, A. J., Araki, T., Sato, A., Tsuda, T., and Yumoto, K.: Oxygen ion uplift and satellite drag effects during the 30 October 2003 daytime superfountain event, Ann. Geophys., 25, 569–574, https://doi.org/10.5194/angeo-25-569-2007, 2007.

Tsurutani, B. T., Verkhoglyadova, O. P., Mannucci, A. J., Saito, A., Araki, T., Yumoto, K., Tsuda, T., Abdu, M. A., Sobral, J. H. A., Gonzalez, W. D., McCreadie, H., Lakhina, G. S., and Vasyliunas, V. M.: Prompt penetration electric fields (PPEFs) and their ionospheric effects during the great magnetic storm of 30–31 October 2003, J. Geophys. Res., 113, A05311, https://doi.org/10.1029/2007JA012879, 2008a.

Tsurutani, B. T., Echer, E., Guarnieri, F. L., and Kozyra, J. U.: CAWSES November 7–8, 2004, superstorm: Complex solar and interplanetary features in the post-solar maximum phase, Geophys. Res. Lett., 35, L06S05, https://doi.org/10.1029/2007GL031473, 2008b.

Valladares, C. E., Villalobos, J., Hei, M. A., Sheehan, R., Basu, S., MacKenzie, E., Doherty, P. H., and Rios, V. H.: Simultaneous observation of travelling ionospheric disturbances in the Northern and Southern Hemispheres, Ann. Geophys., 27, 1501–1508, https://doi.org/10.5194/angeo-27-1501-2009, 2009.

Verkhoglyadova, O. P., Tsurutani, B. T., Mannucci, A. J., Mlynczak, M. G., Hunt, L. A., Komjathy, A., and Runge, T.: Ionospheric VTEC and thermospheric infrared emission dynamics during corotating interaction region and high-speed stream intervals at solar minimum: 25 March to 26 April 2008, J. Geophys. Res., 116, A09325, https://doi.org/10.1029/2011JA016604, 2011.

Verkhoglyadova, O. P., Tsurutani, B. T., Mannucci, A. J., Mlynczak, M. G., Hunt, L. A., and Runge, T.: Variability of ionospheric TEC during solar and geomagnetic minima (2008 and 2009): ex-

ternal high speed stream drivers, Ann. Geophys., 31, 263–276, https://doi.org/10.5194/angeo-31-263-2013, 2013.

Wei, Y., Hong, M., Wan, W., Du, A., Lei, J., Zhao, B., Wang, W., Ren, Z., and Yue, X.: Unusually long lasting multiple penetration of interplanetary electric field to equatorial ionosphere under oscillating IMF Bz, Geophys. Res. Lett., 35, L02102, https://doi.org/10.1029/2007GL032305, 2008.